

Active primary mirror support for the 2.1-m telescope at the San Pedro Mártir Observatory

L. Salas, L. Gutiérrez, M. H. Pedrayes, J. Valdez, C. Carrasco, M. Carrillo, B. Orozco, B. García, E. Luna, E. Ruiz, S. Cuevas, A. Iriarte, A. Cordero, O. Harris, F. Quiroz, E. Sohn, and L. A. Martínez

We have designed and installed a new set of actuators for the suspension of the primary mirror of the 2.1-m telescope at San Pedro Mártir. This active optics system has allowed us to correct low-order aberrations identified by several wave-front analysis techniques. © 1997 Optical Society of America

Key words: Telescope wave-front aberrations, active optics.

1. Introduction

The year of 1989 marked a new era in the design of optical telescopes, when the concept of active optics saw first light in the European Southern Observatory's (ESO's) New Technology Telescope (NTT),¹ and several aberration terms, including a large spherical aberration of $3\ \mu\text{m}$, were corrected to obtain images with 80% of the light contained in a circle of 0.3 arcsec in diameter (d_{80}). Since then, all new telescopes that are constructed incorporate a system of actuators to deform a mirror to cancel optical aberrations. Together with this effort, new methods to quantify the wave-front aberrations have been envisaged.² Another field, adaptive optics, which is closely related to these topics, is also growing rapidly. Old telescopes, however, can also benefit from these new developments, increasing their efficiency, as the square of the image quality, at a moderate cost. In 1994, an effort to correct the 4-m Cerro Tololo Inter-American Observatory (CTIO) telescope in Chile began.³ That mirror is twice as thick as the NTT mirror and is thus eight times stiffer. Nevertheless, Baldwin *et al.*³ pro-

posed that a system of only push actuators still would be enough to correct low-order aberrations. This system, together with other seeing improvement measures, has only slightly improved the image quality.⁴ Although the reason is still unclear, a possibility for this is that the mirror is too stiff for this kind of actuator. At the San Pedro Mártir Observatory we started a similar effort to correct the 2.1-m telescope primary mirror, with the goal of halving the image size to $d_{80} = 0.6''$, thus increasing the efficiency of the telescope by a factor of 4.

2. Mirror and Support

The primary mirror of the 2.1-m telescope⁵ at San Pedro Mártir was made by Owens Illinois in the late 1960's, using Cervite as the blank material. It was polished by Norman Cole in 1976 to a focal ratio of 2.27. The mirror was suspended in its cell by an air bag, with the pressure controlled pneumatically by a cosine gravity regulator, built by Boller & Chivens, and with lateral support provided by a mercury belt. Classical standards in mirror technology dictate a 1/6 width-to-diameter ratio. However, the 2.1-m telescope was conceived as a lightweight (2 ton) mirror, being only 26 cm thick at the edge, which is almost as thin as the NTT mirror.¹

The 2.1-m telescope at San Pedro Mártir (SPM) saw first light in 1979 and was commissioned to the National Observatory of Mexico, an affiliation of the Institute of Astronomy of the National University of Mexico (UNAM). The image quality was accepted as reasonable for a number of years, until the advent of solid-state detectors and active optics. Astigmatism was identified as the main aberration, with a

A. Cordero is with the Universidad Autónoma de Puebla, Apdo. Postal 1152, 72000 Puebla, Puebla, México. C. Carrasco and M. Carrillo are with the Universidad Autónoma de Baja California, Carretera Tijuana-Ensenada, Km 103, CP 22870, B. C., México. All other authors are with the Instituto de Astronomía, Universidad Nacional Autónoma de México, P.O. Box 439027, San Ysidro, California 92143-9027.

Received 8 March 1996; revised manuscript received 3 September 1996.

0003-6935/97/163708-09\$10.00/0

© 1997 Optical Society of America

rms of 0.5 μm and producing a d_{80} of the order of 1.8 arcsec.

A passive support system is intended to support the mirror for its own weight. The position of the support pads is optimized to obtain a minimum residual deformation of the mirror surface.^{6,7} In an active system, the supports become actuators. These actuators allow the introduction of deformations on the mirror to correct optical aberrations on the wave front. The position of the actuators can be further optimized to target specific kinds of aberration.⁸ The question concerning the number of supports and their positions can be addressed as follows. With the use of thin-plate theory, Nelson⁷ has argued that the rms bending for a thin mirror resting on N supports scales as

$$\delta_{\text{rms}} = \gamma_N \frac{q}{D} \left(\frac{A}{N} \right)^2, \quad (1)$$

where

γ_N is the factor depending on the geometry of the supports (of the order of 10^{-3}),
 q is the applied force (or weight) per unit area,
 D is the $Eh^3/12(1 - \nu^2)$ flexural rigidity,
 ν is the Poisson ratio,
 E is Young's modulus,
 A is the area of the mirror,
 N is the number of support points, and
 h is the height of the mirror.

This relation allows us to have a rough estimate of the mean deformations in the mirror, which are mainly due to the mirror's hanging between supports. Additional deformations are produced by shear forces at the position of the supports. These can increase the mean bending deformations by a factor of 2, but they are reduced substantially when the size of the supporting pad is increased.⁸ To decide the number of supports and their area for the 2-m telescope, we start by comparing the case of the 2-m telescope to that of the NTT. The factor q/D depends only on h for a given material (as h^{-2}). This is almost the same (0.8 difference) for the two mirrors. The factor $(A/N)^{-1}$ is the density of the supports, which can be related to the mean separation between them. The expression for δ_{rms} is derived by considering point supports. However, their size must have a large effect when they deviate from small pads. As an example, a single air bag ($N = 1$), the size of the primary mirror, is capable of supporting the mirror adequately (small δ_{rms}). We propose that increasing the area of the supports has the effect of decreasing the mean distance between them, in such a way that the effective unsupported area should replace A above, so $A = A_m - NA_b$, where A_m is the area of the mirror and A_b is the area of a pad. In this way, a set of 18 actuators, 33 cm in diameter, can provide the same rms deflections as the NTT support system with 78 actuators. In contrast, the size of the pads should

have no effect on the deformations of the mirror at large distances compared with the size of the pads, according to Saint Venant's principle of elasticity.⁸ Because our main target is to control astigmatism in the 2-m mirror, the scale of distances under consideration is 100 cm. Furthermore, increasing the size of the pads has the double advantage of decreasing the effect of shear forces and decreasing the complexity of the pneumatic system, because lower pressures are required.

The 18 actuators are accommodated mainly on two concentric rings, six on the inner ring and 12 on the outer ring. The multiplicity on the outer ring (12) allows us to induce and correct deformations of azimuthal frequency 2 and 3, such as astigmatism and triangular coma, according to their Zernike expansions.⁹ In the radial direction, two actuators are not enough to induce high-order aberrations, such as sphericity, but radial orders of 2 and 3 should be controllable. As to the amount of astigmatism that could be corrected, Schwesinger⁶ has shown that the deflections in a mirror scale with $R^4 \rho g / Eh^2$ when different support systems or force patterns are applied. This factor is 13 times larger for the NTT mirror than for the 2-m telescope mirror, and it limits the number of deformations that can be induced. For the NTT, 500 nm of astigmatism are produced by applying forces that range peak to peak 3% of the value needed to support the weight.¹⁰ This same value would increase to 39% in our case. This range of forces is easy to provide and to control to a 1% level with only push actuators to zenithal distances of up to 2.5 air masses. However, astigmatism requires the lowest energy to be induced or corrected, whereas sphericity is among the aberrations that require more energy to be induced. In the case of the NTT, 500 nm of sphericity require peak to peak forces of 8% to be corrected. This would amount to over a 100% in the 2-m case and could not be provided by only push actuators, even if we had the necessary number of actuators in the radial direction. The system we are proposing is therefore adequate to correct low-order aberrations.

Accordingly, we have selected 18 air bags as actuators, and we have placed them optimally for an even load distribution. Hard points were designed to include load cells and were accommodated within the restrictions posed by the existing design of the mirror cell. Figure 1 shows the position of the actuators and hard points; Fig. 2 shows the computed residual deformations of the mirror that is resting on these supports and the image quality that will be attainable (without atmospheric effects). As we can see, 80% of the flux can be accommodated within a circle of 0.6 arcsec in diameter, which will be the goal for this active system.

3. Control Problem

The purpose of the active system is to control the pressure in each of the 18 actuators (air bags) so that the load carried and the desired deformation and position of the mirror are kept to their desired

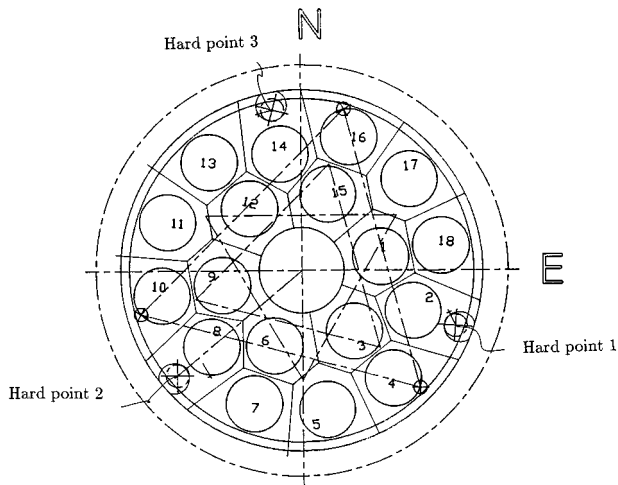


Fig. 1. Position of the 18 force actuators (air bags) and three hard points in the mirror cell.

values. In order to accomplish this, we have divided the control problem into two loops: an internal loop that controls the pressure in each actuator, and an external one that monitors the position of the mirror at the three hard points. An even more external loop, the optical loop, will be closed in the

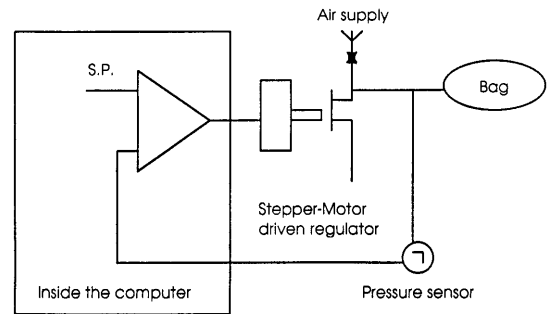


Fig. 3. Pressure control loop regulates the pressure in each air bag to its desired value (set point, S.P.) with better than 1% accuracy. The pressure is controlled through a stepper-motor driven regulator, and a sensor feeds back the actual pressure to the computer.

future. The zenith angle is feed through an inclinometer and a PC-486 computer controls all the hardware and closes the loops. The pressure loop (Fig. 3) consists of a stepper-motor driven air-pressure regulator and a pressure sensor that works in the range 0–3 psi. These elements enable us to control the desired pressure to less than 1% through a proportional algorithm. The cost of each actuator is of the order of \$300.00 (U.S.). The

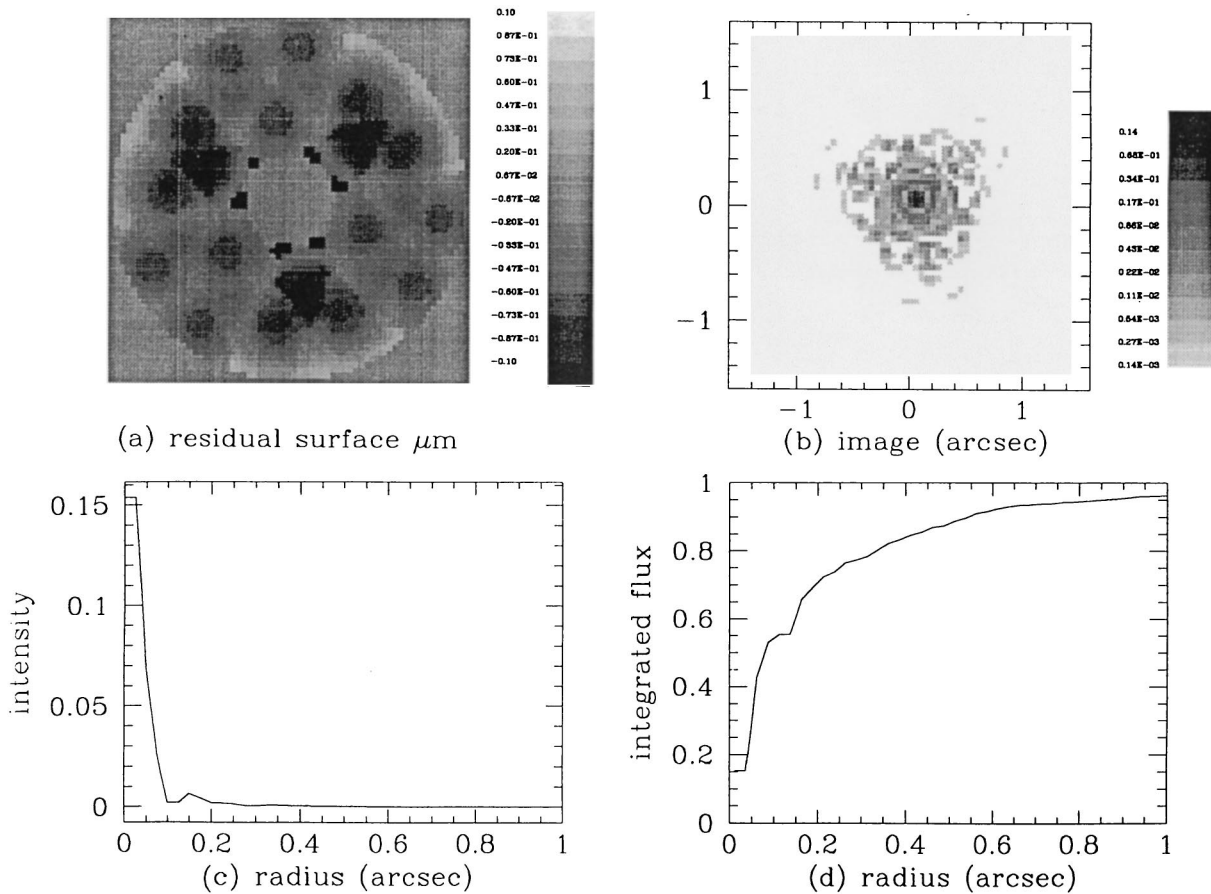


Fig. 2. Calculated residual surface deformation and image quality of the mirror resting in the proposed supports: (a) residual surface deformations; (b) point image produced in focus; (c) intensity distribution of the point image as a function of radius; (d) integrated flux of the point image as a function of radius, showing that 80% of the radiation will be included in a circle of 0.6 arcsec.

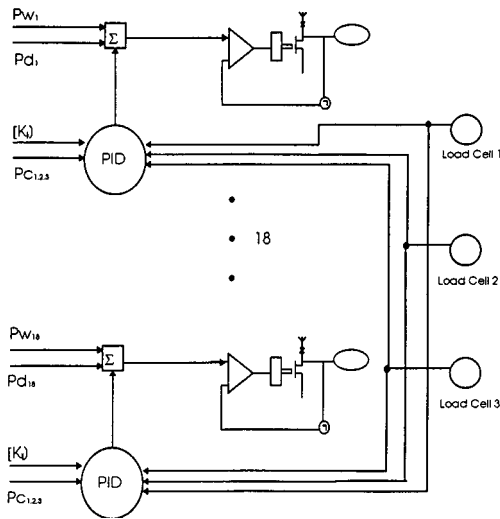


Fig. 4. Position loop modifies the set point of each pressure loop as a function of the fraction of the mirror weight corresponding to each bag (P_{w_i}), the fraction of the mirror weight corresponding to each load cell ($P_{C_{1,2,3}}$), the transformation matrix (K_{ij}) that defines a pressure plane, and the desired deformation (P_{d_i}). A PID algorithm is used to close the position loop. The zenith reference is given by an inclinometer.

position loop (Fig. 4) senses the weight at the three hard points (using load cells) and decides how the pressures at the actuators are to be changed in order to keep the load to its desired value of 13 kg at zenith, through a propagation matrix and a proportional, integral, and derivative (PID) algorithm. The design of the hard points (Fig. 5) decouples lateral movements through a spherical contact

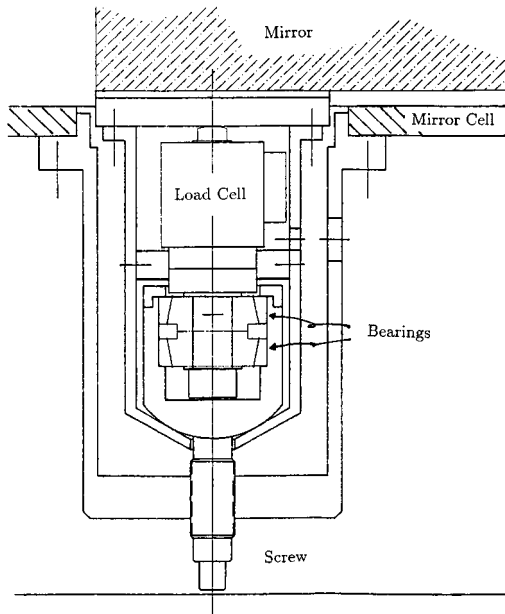


Fig. 5. Mechanical design of the hard points. A load cell senses the weight of the mirror through a spherical contact point. A couple of bearings permit rotatory action to position the height of the mirror at each hard point.

point and allows us to set the height of the hard points through a system of axial bearings that decouple rotatory action. The high stiffness of these hard points ($\approx 0.1 \mu\text{m/kg}$) allows us to infer the position from the load value, with a negligible tilt error. The hard points were precisely machined in our mechanical shop from monolithic pieces of stainless steel.

Because the actuators are air bags they can be modeled by springs of very low stiffness. The problem of the support system then becomes that of a rigid body's reacting on three hard points and being deformed by a set of soft actuators, so that the actuators are not coupled. This is not the case of a mirror resting on hard actuators, such as piezoelectric actuators, for which all actuators are coupled. In our case, as the pressure in one actuator changes, say to introduce a small deformation on the mirror, the pressure in all others is maintained, so the main change of load occurs at the position of the hard points. The load at the hard points can then be balanced by changing the pressure in all the actuators in an organized way. The required pressure can easily be calculated. Because the load at the three hard points defines a plane of pressures, the additional pressure needed to tilt the plane in the opposite direction is obtained by solving the plane equation at the position of the actuators.

The pressure in each actuator consists of three terms, i.e., one to support the weight of the mirror, one to perform the desired deformations, and a third term to correct the pressure based on the weight supported by each of the hard points, as follows:

$$P_i = P_{w_i} \cos z + P_{d_i} + \text{PID} \left(\sum_j K_{i,j} E_{p_j} \right);$$

$$i = 1 \dots 18, j = 1 \dots 3. \quad (2)$$

In Eq. (2), P_i stands for the desired pressure in each actuator, P_{w_i} is the pressure to support each portion of the mirror at zenith, z is the zenith angle, P_{d_i} is the desired deformation pressure; and PID is a proportional, integral, and differential algorithm that corrects the pressure based on the error at each hard point E_{p_j} and a propagation function $K_{i,j}$. The propagation function has been taken to be a plane defined by the error at each hard point, evaluated at the position of the actuators, and weighted by the portion of mirror that each actuator supports (P_{w_i}/M_{tot}). In this manner, an uneven error of support at the hard points results in a pressure change at the actuators that tilts the mirror as a rigid body. The error at each hard point, in turn, has the following form:

$$E_{p_j} = M_j^c - (P_{w_j^c} \cos z + P_{d_j^c}); j = 1 \dots 3, \quad (3)$$

where the c superscript denotes a load cell, M_j^c is the measured pressure on a load cell, and the interpretation of the rest of the terms is as before, namely, the calculated weight that a cell should be standing, and

the desired deformation at the position of the hard points. The high stiffness of the load cells allows us to use the hard points as actuators without introducing a significant tilt to the mirror. The control system monitors the pressure at each actuator (M_i) and provides a proportional correction to reach the desired pressure P_i .

4. Installation and Optical Testing

The active system for the 2.1-m telescope was installed and tested during a 10-day period in September 1995. Three different methods were used to test and quantify optical aberrations; one of them used a bi-Ronchi ruling test¹¹ and the other two followed the curvature sensing approach.^{2,12}

The Ronchi test can be used to obtain the optical path difference or phase in an arbitrary wave front by obtaining two Ronchigrams that orient the slit in two perpendicular directions.¹³ The experimental setup consists of a Ronchi ruling located in the converging beam of the telescope, followed by a lens in the focal plane that images the exit pupil on the detector. A star is used as the light source for this test. In order to obtain information about the two axes simultaneously, a bi-Ronchi or squared ruling can be used instead of a single ruling.¹¹ This ruling represents the intersection of two perpendicular Ronchi rulings, and the dots obtained in the pattern at the detector can be interpreted as the intersection of two separate Ronchigrams.

Given x and y , the coordinates of the centroids of the dots belonging to the Ronchigram in the exit pupil, we perform a polynomial fit for the transverse aberrations T_x and T_y , as

$$T_x = \sum_{i=0}^{k-1} \sum_{j=0}^i C_{ij} x^j y^{i-j}, \quad (4a)$$

$$T_y = \sum_{i=0}^{k-1} \sum_{j=0}^i D_{ij} x^j y^{i-j}, \quad (4b)$$

where $k - 1$ is the polynomial degree. The coefficients C_{ij} and D_{ij} are obtained by performing two least-squares fits; the first one solves independently for x and y is used as a starting solution for the second fit, which solves the crossed Ronchigram.

As in a Hartmann test, the transverse aberrations are related to the wave front by

$$\frac{\partial W}{\partial x} = -\frac{T_x}{R}, \quad \frac{\partial W}{\partial y} = -\frac{T_y}{R}, \quad (5)$$

where R is the curvature radius of the wave front in the exit pupil. If we express W at the exit pupil by a similar polynomial expansion,

$$W(x, y) = \sum_{i=0}^k \sum_{j=0}^i B_{ij} x^j y^{i-j}, \quad (6)$$

and substitute back, we obtain a system of equations that relates coefficients C_{ij} and D_{ij} to B_{ij} , from which the B_{ij} are calculated. Finally, W is further ex-

pressed in terms of a linear combination of Zernike polynomials.¹⁴

The curvature sensing method² allows us to reconstruct the aberrated wave front from a measure of two out of focus images of a star, obtained at the telescope by moving the detector in and out of the focal plane. From these two images (I_1 and I_2), a curvature measurement is obtained as

$$C = \frac{I_1 - I_2}{\frac{1}{2}(I_1 + I_2)}, \quad (7)$$

which can be related to the sensor signal,²

$$S(\rho, \theta) = \frac{1}{I} \frac{\partial I}{\partial z} \frac{f(f-l)}{l}. \quad (8)$$

Here f is the focal length and l is the position at which out-of-focus images are obtained.²

This signal is used to derive the wave front by means of the irradiance transport equation,

$$\frac{\partial I}{\partial z} = -(\nabla I \cdot \nabla W + I \nabla^2 W), \quad (9)$$

where the nabla are partial derivatives in the plane perpendicular to z , which is the direction of beam propagation. Two methods have been used in this study to solve this equation: the one proposed by Roddier,² and the one proposed by Salas.¹² The first method solves the irradiance transport equation as a second-order difference equation with Neuman boundary conditions, and it then performs a least-squares fit to a Zernike polynomial expansion. The second method substitutes a Zernike polynomial expansion directly into the irradiance transport equation, and it makes use of the cylindrical symmetry of the problem to decouple the radial and azimuthal components into a radial Zernike and a Fourier series, respectively, solving the azimuthal part directly by a Fourier transform and the radial part by a one-dimensional polynomial fit.

We tested several configurations of pressures applied to the back of the mirror through the set of 18 actuators. To illustrate the operability of the system, we show the result of applying a pattern of forces aimed primarily at correcting astigmatism. We have measured the deformations obtained at the position of the actuators that are due to this pattern of force. This measurement is the difference of the original (uncorrected) wave front and the wave front obtained after the force pattern was modified. In Fig. 6 we show these wave fronts [(a), original; (b), modified; and (c), difference]; Fig. 6(d) shows the pattern of pressures used to deform the mirror. The wave fronts in this figure were obtained by the variable separation in the curvature sensing method.¹² As we can see, there is a close relation between the obtained deformations [Fig. 6(c)] and the pattern of applied forces [Fig. 6(d)]. This is expressed better in Fig. 7, where we see a linear dependence of the obtained deformation on the applied pressure at the

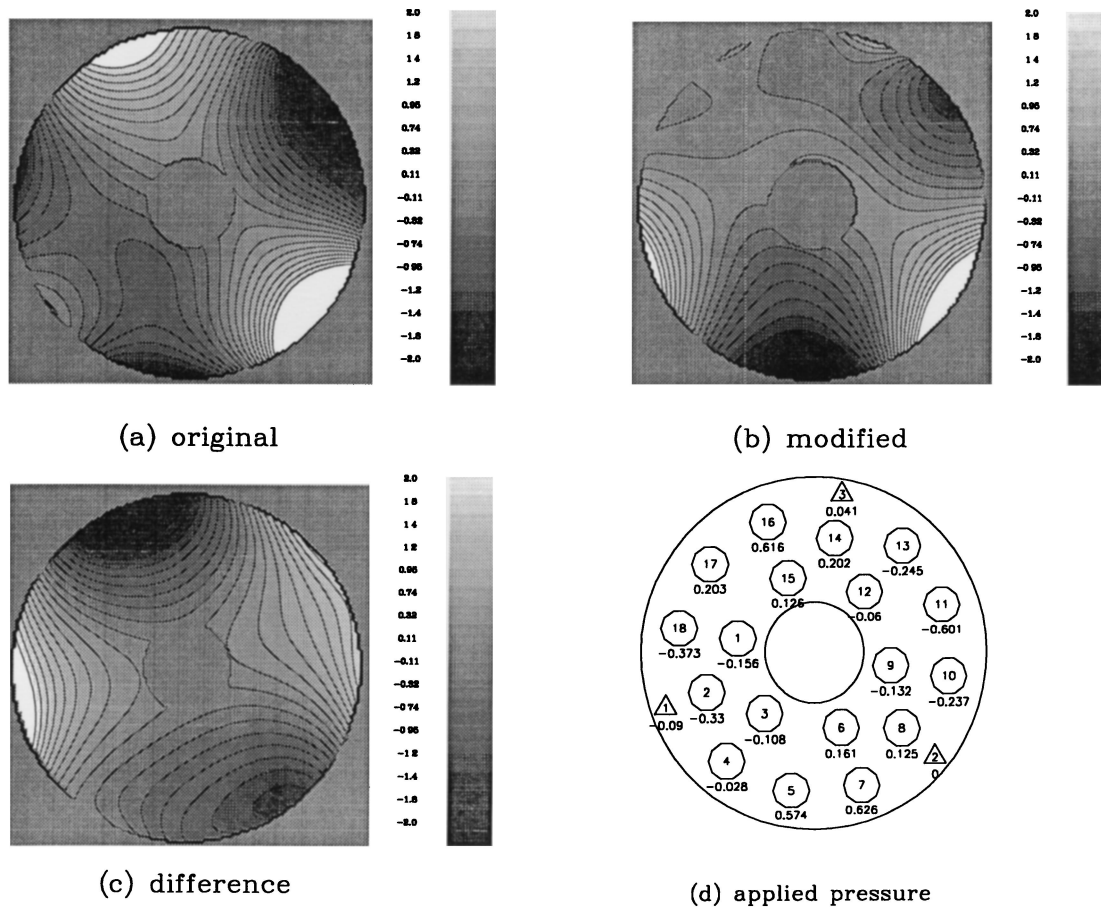


Fig. 6. Effect of applied pressures on the wave front: (a) original wave front (μm); (b) wave front obtained after pressures were applied to the actuators; (c) the difference of (b) - (a); (d) the set of applied pressures in each actuator.

position of each actuator (actuators are numbered in this graph). Three actuators deviate from this relation; this result is probably due to the dissimilar value of the pressure there to its surroundings. These three actuators had values in excess of the pure astigmatism correction, which prompts in the

'direction of different relations for different modes being corrected.

Roddier *et al.*¹⁵ have measured aberrations in a number of telescopes by using the curvature sensing approach.² They were kind enough to allow us to use their program to test our telescope. In Table 1

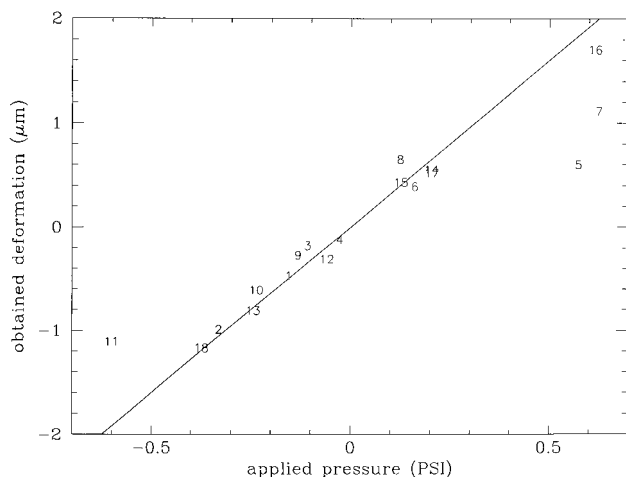


Fig. 7. Graph of the deformations obtained at the position of the actuators versus the applied pressure. Each actuator is numbered. The solid line represents a slope of 3 $\mu\text{m}/\text{psi}$.

Table 1. Intrinsic rms Aberrations of Different Telescopes

Aberration ^a	Average ^b	NTT ^c (1992)	SPM 2 m		
			<i>f</i> /7.5 (1994)	<i>f</i> /7.5 (9/12/95)	<i>f</i> /13.5 (9/14/95)
Astigmatism	213	202	500	164	6
Coma	186	296	59	142	
Triangular	84	72	35	71	98
Quadric	48	31	33	86	3
Z_{11}	73	50	-112	-1	
Spherical	64	30	70	-75	-2
Total	408	218	604	300	216
Resid.(-25Zer)	73	66	85	38	

^aSpherical aberration refers to the addition of terms Z_{11} and Z_{22} .

^bThis is the average of ten different telescopes (United Kingdom Infrared, Infrared Telescope Facility, Canada-France-Hawaii, University of Hawaii 88 in., NTT, CTIO 4 m, Hale 5 m, 3.6 European Southern Observatory, Hubble Space, Nordic Optical), as given in Ref. 15.

^cThe aberrations of the NTT obtained in Ref. 2 are shown with the introduction of a known coma term.

PSF

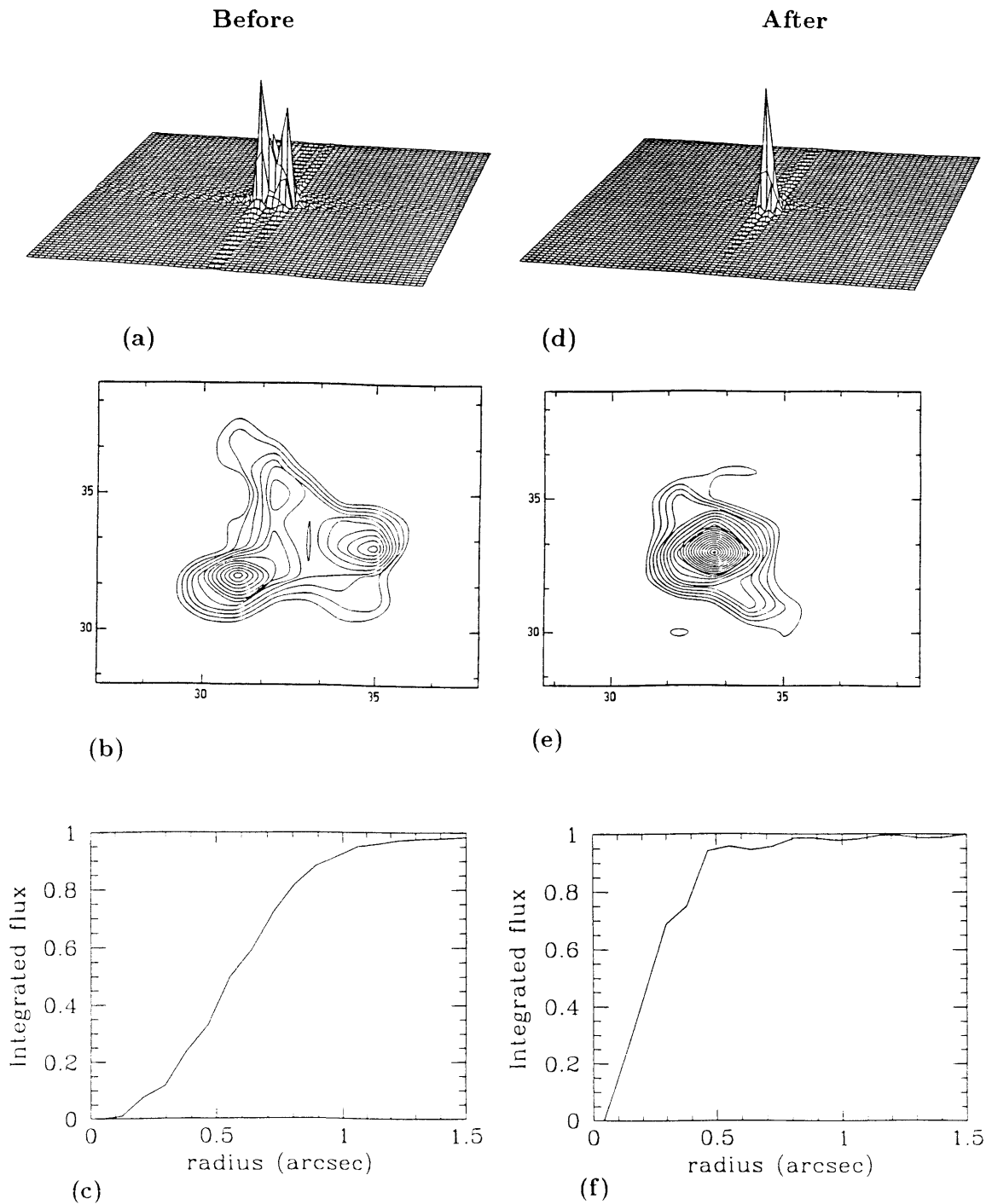


Fig. 8. PSF reconstructions from wave-front analyses, before [(a)–(c)] and after [(d)–(f)] the introduction of the active system; (a) and (c) show surface plots of the PSF, (b) and (e) show contour plots with a scale of 0.15 arcsec per pixel, and (c) and (f) show the integrated flux contained in a circle of radius r .

we show the comparison of the mean of ten telescopes, the NTT, and the 2.1-m SPM telescope, before and after the introduction of the active system in September 1995 (in its two secondary configurations, $f/7.5$ and $f/13.5$). It is important to note that all the measurements in this table were obtained with the

same program. Astigmatism has largely been reduced, to the point where the total aberration is comparable with that of the NTT and much better than the mean value.

The point spread function (PSF), which used to have three peaks as a result of coma and astigma-

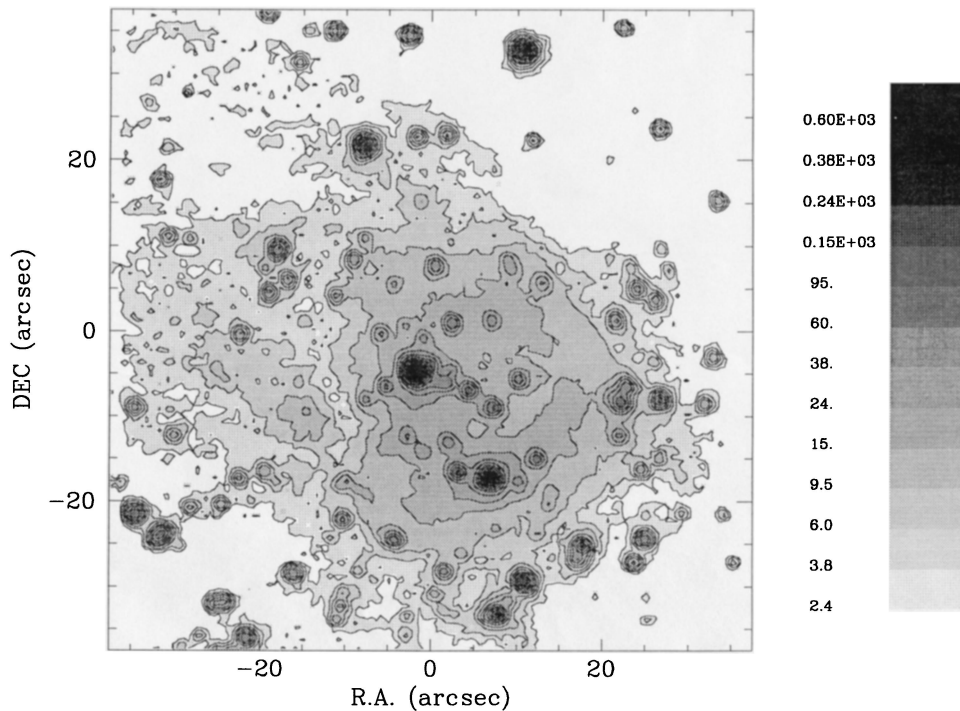


Fig. 9. Image of the Ultra-Compact HII region G173.7, obtained with the corrected $f/13$ configuration and the infrared camera CAMILA. Contours are log spaced with 0.2 decimal exponent intervals. The offset position from the central source is given in arcseconds for declination (DEC) and right ascension (R.A.).

tism, now has a single peak, as we can see by the PSF reconstructions in Fig. 8, obtained with the wave-front bi-Ronchi analysis.¹¹ A d_{80} of $0.9''$ has already been obtained, close to the goal of $0.6''$.

As of November 1995, while we were still in the process of learning to control mixed order aberrations and improving local seeing conditions, images of up to 0.7 arcsec were already being reported (M. Tapia, personal communication). The image quality is exemplified by a $2\text{-}\mu\text{m}$ image of the Ultra-Compact HII region,¹⁶ G173.7 (Fig. 9), obtained with the infrared camera CAMILA¹⁷ in the $f/13.5$ configuration.

5. Conclusions

We have performed an active control system for the primary mirror of the 2.1-m telescope at the San Pedro Mártir Observatory. The system has shown its capabilities in the correction of astigmatism, and higher modes of correction await more detailed studies.

We thank all the personnel at the SPM Observatory for their strong support during the installation phase, as well as the headquarters personnel in Ensenada City. In particular we are indebted to A. Córdoba, G. Sierra, S. Monroy, A. Sarabia, J. M. Murillo, F. Martínez, A. Meling, R. Graef, I. González, E. López, J. L. Ochoa, and J. C. Avelar. We are also indebted to F. Roddier and C. Roddier for lending us their curvature sensing program to test and compare our results.

References

1. R. N. Wilson, F. Franza, L. Noethe, and G. Andreoni, "Active optics IV. Set-up and performance of the optics of the ESO New Technology Telescope (NTT) at the observatory," *J. Modern Opt.* **38**, 219–243 (1991).
2. C. Roddier and F. Roddier, "Wave-front reconstruction from defocused images and the testing of ground-base optical telescopes," *J. Opt. Soc. Am. A* **10**, 2277–2287 (1993).
3. J. Baldwin, G. Pérez, B. Gregory, W. Weller, R. Wilson, and L. Noethe, "Retrofitting new technology to an old telescope," in *ESO Conference on Progress in Telescope and Instrumentation Technologies* (European Southern Observatory, Garching, Germany, 1992), pp. 247–250.
4. J. Baldwin, "4-m image quality improvements," *Natl. Opt. Astron. Observ. Newslett.* **41**, 34–35 (1995).
5. J. de la Herrán, "The Mexican 2.12-m telescope for the National Astronomical Observatory at SPM, BC, México," in *Symposium on Recent Advances in Observational Astronomy Held at Ensenada, México* (UNAM Press, México City, 1981), pp. 133–139.
6. G. Schwesinger, "Theoretical aspects of mirror support," in *Proceedings of the Symposium on Support and Testing of Large Astronomical Mirrors* (U. of Arizona Press, Tucson, Ariz., 1968), pp. 11–46.
7. J. E. Nelson, J. Lubliner, and T. S. Mast, "Telescope mirror supports: plate deflections on point supports," in *Advanced Technology Optical Telescopes I*, L. D. Barr and G. Burbidge, eds., *Proc. SPIE* **332**, 212–228 (1982).
8. L. Arnold, "Uniform load and actuator influence functions of a thin or thick annular mirror. Application to active mirror support optimization," *Appl. Opt.* **35**, 1095–1106 (1996).
9. M. Born and E. Wolf, *Principles of Optics*, 5th ed. (Pergamon, Oxford, 1975), Chap. 9, p. 464.
10. R. N. Wilson, F. Franza, and L. Noethe, "Active optics I. A

- system for optimizing the optical quality and reducing the costs of large telescopes," *J. Mod. Opt.* **34**, 485–509 (1987).
11. A. Cordero, E. Luna, S. Zárate, and O. Harris, "Evaluación de la calidad de la imagen del telescopio de 2.1-m," Tech. Rep. 95-02 (Instituto de Astronomía, UNAM Press, Mexico City, 1995).
 12. L. Salas, "Variable separation in curvature sensing. A fast method to solve the irradiance transport equation in the context of optical telescopes," *Appl. Opt.* **35**, 1593–1596 (1996).
 13. A. Cornejo, "Ronchi test," in *Optical Shop Testing*, 2nd ed., D. Malacara, ed. (Wiley, New York, 1991), pp. 338–339.
 14. D. Malacara and L. DeVore, "Interferogram evaluation and wavefront fitting," in *Optical Shop Testing*, 2nd ed., D. Malacara, ed. (Wiley, New York, 1991), pp. 470–472.
 15. C. Roddier, J. E. Graves, M. J. Northcott, and F. Roddier, "Testing optical telescopes from defocused stellar images," in *Advanced Technology Optical Telescopes V*, L. M. Stepp, ed., Proc. SPIE **2199**, 1172–1177 (1994).
 16. M. Miralles, S. Kurtz, I. Cruz-González, and L. Salas, Instituto de Astronomía, UNAM, Ensenada 22800, México (personal communication, 1996).
 17. I. Cruz-González, L. Carrasco, E. Ruiz, L. Salas, M. Skrutskie, M. Meyer, P. Sotelo, F. Barbosa, L. Gutiérrez, A. Iriarte, F. Cobos, A. Bernal, B. Sánchez, J. Valdéz, S. Argüelles, and P. Conconi, "CAMILA: Infrared Camera/Spectrograph for OAN-SPM," in *Instrumentation in Astronomy VIII*, D. L. Crawford and E. R. Craine, eds., Proc. SPIE **2198**, 774–780 (1994).